Geometric Ginzburg-Landau theory for faceted crystals in one dimension: From coarsening to chaos through a driving force

Frank Haußer*
Fachbereich II—Mathematik, Technische Fachhochschule Berlin, Luxemburger Straße 10, 13353 Berlin, Germany

Axel Voigt†
Institut für Wissenschaftliches Rechnen, Technische Universität Dresden, Zellescher Weg 12-14, 01062 Dresden, Germany
(Received 3 September 2008; published 14 January 2009)

We consider the dynamic behavior in driven phase transitions dominated either by attachment-detachment or by surface diffusion mass transport mechanisms. As the driving force increases, we numerically demonstrate for both cases that the spatiotemporal faceted structure of the surface undergoes a sequential transition from slow coarsening turning to accelerated coarsening followed by fixed length scale structures before finally becoming spatiotemporally chaotic. For the attachment-detachment dominated phase transition problem we compare in the accelerated coarsening regime the simulation results with an intrinsic dynamical system governing the leading-order piecewise-affine dynamic surface (PADS), which can be obtained through a matched asymptotic analysis. The PADS predicts the numerically observed coarsening law for the growth in time of the characteristic morphological length scale $\mathcal{L}_{\mathcal{M}}$. In particular we determine the prefactor of the scaling law which allows for quantitative predictions necessary for any use of the theory in preparing patterned surfaces through modifications of the driving force.

DOI: 10.1103/PhysRevE.79.011115 PACS number(s): 05.70.Np, 05.45.−a, 68.55.−a, 81.10.Aj

I. INTRODUCTION

Driven self-assembly, which naturally arises in a variety of material science problems when bulk and surface energy interact, offers new and rich possibilities in both theory and applications. The self-organizing ensembles of nanofaceted pyramids is a prominent example which has been extensively studied in recent years. A promising approach to describe the self-assembly is to use an effective nonconvex surface free energy which leads to spinodal decomposition of unstable surface orientations into faceted structures with stable orientations [1,2]. The nonconvexity of the effective surface energy corresponds to a strongly anisotropic surface tension leading to a negative surface stiffness for certain ranges of surface orientations. Therefore the corresponding evolution equations become ill-posed unless the additional energy of edges and corners is included, which does lead to the dependence of the surface tension on the local curvature [3,4]. However, to date, theoretical and computational studies of the associated surface dynamics have generally been limited to long-wave approximations based on small variations in surface orientation [5–9]. This introduces a clear limit to the quantitative predictive power of the theory in relation to large classes of experimentally observed morphologies, such as facets which meet at high angles of incidence [10–12].

In this paper, we present a computational study of the coarsening-to-chaos transition of two representative driven phase-ordering models of a thermodynamically unstable crystal surface. The models arise from attachment-limited growth and growth governed by surface diffusion. We will not employ any long-wave approximation and therefore are able to explore the full geometric theory.

*hausser@tfh-berlin.de
†axel.voigt@tu-dresden.de

II. GEOMETRIC MODEL

We consider two types of surface evolutions, which are given in nondimensional form terms of a nondimensional thermodynamic surface free energy E and a nondimensional driving force ε as

$$\mathcal{V}_n = -\frac{\delta E}{\delta \mathcal{I}} + \varepsilon, \tag{1}$$

$$\mathcal{V}_n = \Delta_{\mathcal{I}} \frac{\delta E}{\delta \mathcal{I}} + \varepsilon, \tag{2}$$

where $\mathcal{V}_n$ denotes the normal velocity of the crystal surface $\mathcal{I}$, $\delta E/\delta \mathcal{I}$ denotes the functional derivative with respect to normal variations of the surface $\mathcal{I}$, and $\Delta_{\mathcal{I}}$ is the surface Laplacian. The phenomenological equation (1) can be used to describe attachment-detachment kinetics and can serve as a simplified model for the interface evolution in liquid phase epitaxy (LPE) or electrodeposition [13]. If the dominant mass transport mechanism is surface diffusion along the surface, Eq. (2) can be used as a phenomenological model, e.g., as a simplified surface model for chemical vapor deposition (CVD) [8]. In the case of attachment detachment kinetics, the driving force ε is proportional to the difference between the chemical potentials of the bulk phases, reflecting the interaction of bulk energy with the surface. For the surface diffusion dynamics, the driving force usually originates from a deposition flux. Note that in both cases we are assuming that the resulting material flux (i.e., the driving force) is normal to the surface, which is due to the effect of a diffusion boundary layer whose shape follows the shape of the surface. This is in contrast to other growth mechanisms, e.g., molecular beam epitaxy (MBE), where the deposition flux does not follow the morphology of the surface. As pointed out in Ref.

[9], in the latter case the driving force may be eliminated by changing to a frame of reference comoving with the flat surface perpendicular to the deposition flux and therefore the strength of the driving force has no influence on the morphology of the surface in that case.

The dimensionless thermodynamic surface free energy is defined through

$$E[\mathcal{I}] = \int_{\mathcal{I}} \left(\gamma(\mathbf{n}) + \frac{1}{2}\kappa^2 \right) dS, \tag{3}$$

with γ denoting an effective nonconvex surface free energy density depending on the local orientation $\mathbf{n}$ and κ being the mean curvature. The curvature term models an edge energy which is concentrated in the region where two stable facets meet [3,4]. Note that the facets are due to the nonconvexity and not due to cusps in the surface free energy. The curvature term arises most naturally as the first order term in the expansion of a general surface free energy density, which for a one-dimensional (1D) surface is given by $\hat{\gamma}(\theta, \partial_s\theta, \ldots)$ [3], θ denoting the local tangent angle and s denoting the arc length along the surface. The models thus define a geometric Ginzburg-Landau theory for the morphology of crystal surfaces, where γ corresponds to a double well potential and the curvature term to the gradient term. With $\epsilon=0$, Eq. (1) is the geometric analog of a nonconserved Allen-Cahn–type evolution law, whereas Eq. (2) is a geometric version of a conserved Cahn-Hilliard–type evolution law.

For simplicity, we now consider the model system of 1D surfaces with a constant driving force $\varepsilon \geqslant 0$. A direct application for the 1D model is given in the study of self-assembled 2D systems, e.g., Ref. [14].

From Eqs. (1)–(3) we obtain

$$\mathcal{V}_n = \Gamma(\theta)\kappa - \partial_{SS}\kappa - \frac{1}{2}\kappa^3 + \varepsilon, \tag{4}$$

$$\mathcal{V}_n = \partial_{SS}\left(-\Gamma(\theta)\kappa + \partial_{SS}\kappa + \frac{1}{2}\kappa^3 \right) + \varepsilon, \tag{5}$$

respectively, where $\Gamma(\theta) = \gamma(\theta) + \gamma_{\theta\theta}(\theta)$ is the surface stiffness as a function of the local tangent plane angle θ relative to the unstable orientation $\theta=0$ [i.e., $\Gamma(0) < 0$] and $\kappa = \partial_s\theta$ is the curvature.

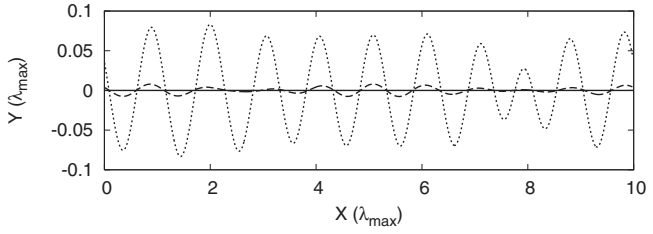

FIG. 1. Spinodal decomposition: The initially flat surface with random perturbation $\sim 10^{-3}$ evolves into a hill-valley structure with wavelength λ_{max}. Surface at time $t=0.0$ (solid), $t=25$ (dashed), and $t=50$ (dotted).

In the nondriven case ($\epsilon=0$), the surface displays an emergent morphology comprising of extended facets, with orientations $\pm\beta$ given to leading order by the Wulff construction for $\gamma(\theta)$, which meet and merge over relatively narrow rounded edges and vertices. The surface also slowly coarsens, and one finds $\mathcal{L}_{\mathcal{M}} \approx \ln t$, for the growth in time t of

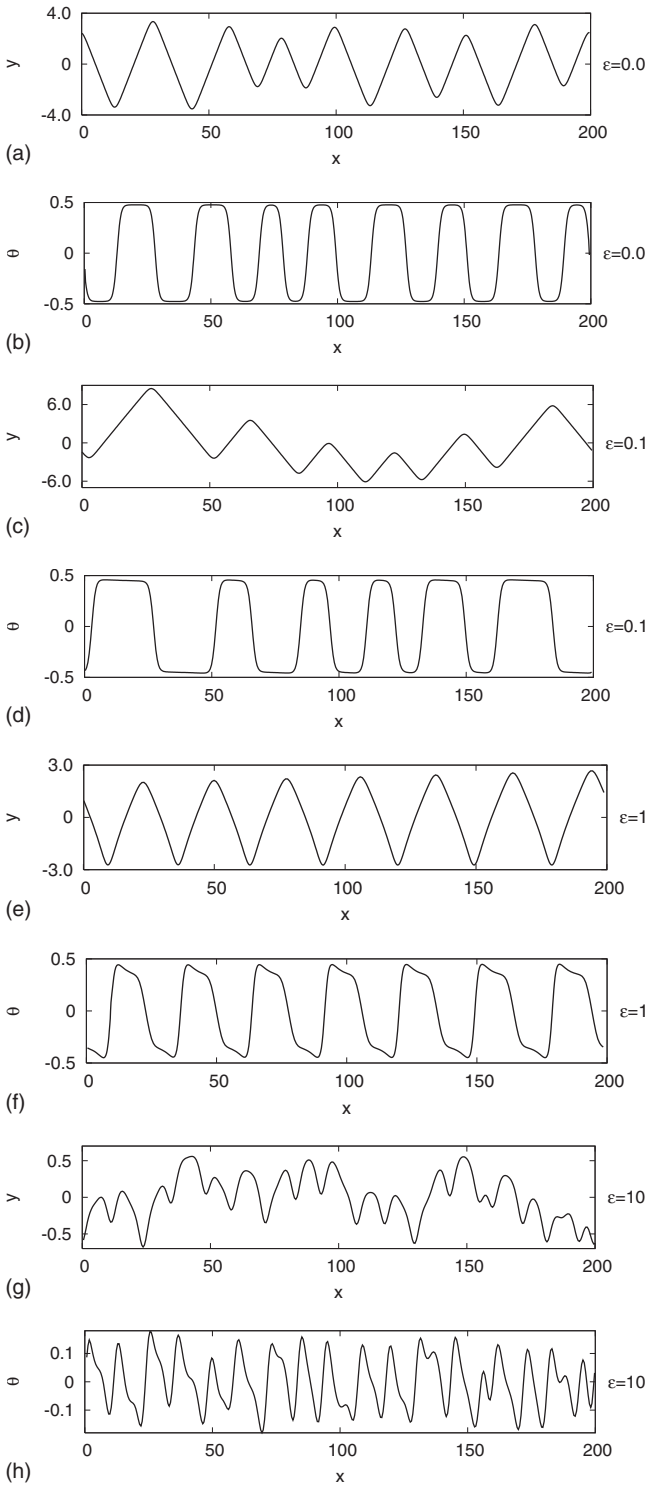

FIG. 2. Numerical simulation of Eq. (4) showing surface and angle at late times for the four different regimes of the driving force ε.

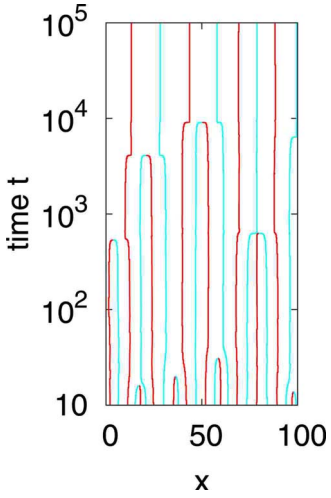

FIG. 3. (Color online) Space-time trajectories of kink [red (black)] and antikink [blue (gray)] positions obtained by numerical simulation of Eq. (6) with $\varepsilon=0$, showing logarithmic slow coarsening via kink-antikink coalescence.

the characteristic facet length scale $\mathcal{L}_{\mathcal{M}}$, which is consistent with the long-wave approximation for both equations. On the other hand, a large driving force $\varepsilon \gg 1$ yields an apparently chaotic spatiotemporal surface evolution. This may be formally understood by first changing to a frame of reference comoving with the flat surface $\theta=0$ at speed ε, yielding in the new coordinates

$$\mathcal{V}_n = \Gamma(\theta)\kappa - \kappa_{\mathrm{SS}} - \frac{1}{2}\kappa^3 + \varepsilon(1-\cos\theta), \tag{6}$$

$$\mathcal{V}_n = \partial_{\mathrm{SS}}\left(-\Gamma(\theta)\kappa + \kappa_{SS} + \frac{1}{2}\kappa^3\right) + \varepsilon(1-\cos\theta), \tag{7}$$

which results from the normal nature of the driving force as a result of the diffusion boundary layer in the bulk phases. Making the transformation $\theta \to \theta/\varepsilon$ and $t \to \varepsilon t$ reduces Eq. (6), in the limit $\varepsilon \to \infty$, to a geometric counterpart of the Kuramoto-Sivashinsky equation, namely,

$$\mathcal{V}_n = \theta^2 - \kappa - \kappa_{\mathrm{SS}}.$$

Below we detail the transition between logarithmic coarsening and chaotic behavior of Eqs. (6) and (7) as one increases the driving force ε.

III. FROM COARSENING TO CHAOS

We probe both the dynamic instability of the initial orientation $\theta=0$ and the resulting nonlinear evolution of the surface morphology for Eqs. (6) and (7) by using an adaptive finite element method [15–17]. Here we use a prototype nonconvex surface energy density γ with stiffness

$$\Gamma(\theta) = 1 - \alpha\cos(4\theta), \quad \text{with } \alpha = 2,$$

leading to minimal stable orientations $\pm\beta \approx 0.48$. We find that small initial perturbations of the surface $\theta=0$ rapidly evolve into essentially a periodic hill-valley structure with wavelength $\lambda = 2\pi\sqrt{2}$; see Fig. 1 for Eq. (6). For Eq. (7), a similar result is shown in Ref. [16], where in that case $\lambda = 2\pi\sqrt{3/2}$. This behavior is consistent with a linear stability analysis of Eqs. (6) and (7), which predicts exponential growth of the Fourier mode with these wavelengths on a time scale t to be the dominant instability. Viewing the angle θ as an order parameter, this behavior is identical to the phase separation of a deeply quenched binary alloy, and is commonly referred to as spinodal decomposition of the unstable surface.

The fully nonlinear surface dynamics that emerges beyond spinodal decomposition display four qualitatively different spatiotemporal signatures as ε increases, see Fig. 2, where the surface and angle at late times for four qualitatively different regimes of the driving force ε in Eq. (6) are displayed. For both Eqs. (6) and (7), in the nondriven case ($\varepsilon=0$) the surface is comprised of extended facets with orientation $\theta \sim \pm\beta$ which meet at relatively narrow rounded valleys (kinks) and hill tops (antikinks). The space-time plot

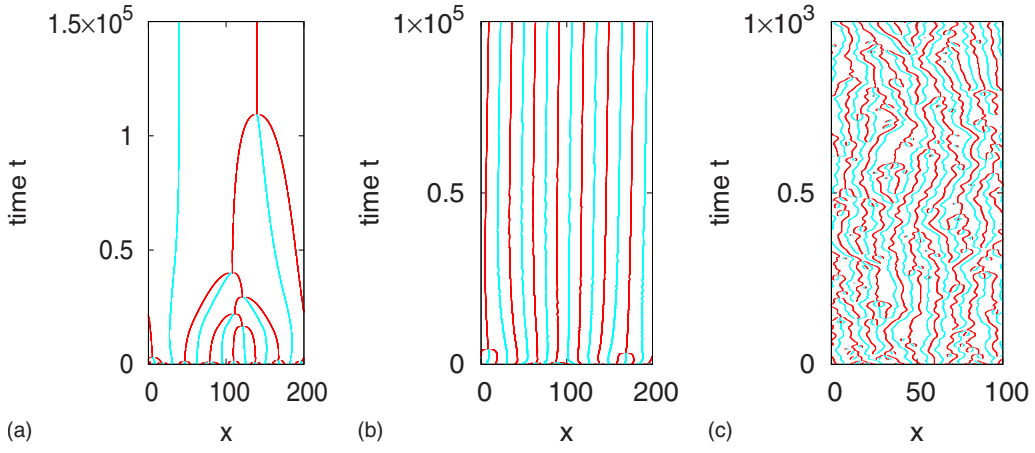

FIG. 4. (Color online) Space-time trajectories of kink [red (black)] and antikink [blue (gray)] positions obtained by numerical simulation of Eq. (6). (Left to right) $\varepsilon=0.1$: fast coarsening via kink-antikink-kink coalescence. $\varepsilon=1.0$: interrupted coarsening, fixed length scale structure as steady state. $\varepsilon=10.0$: irregular dynamics.

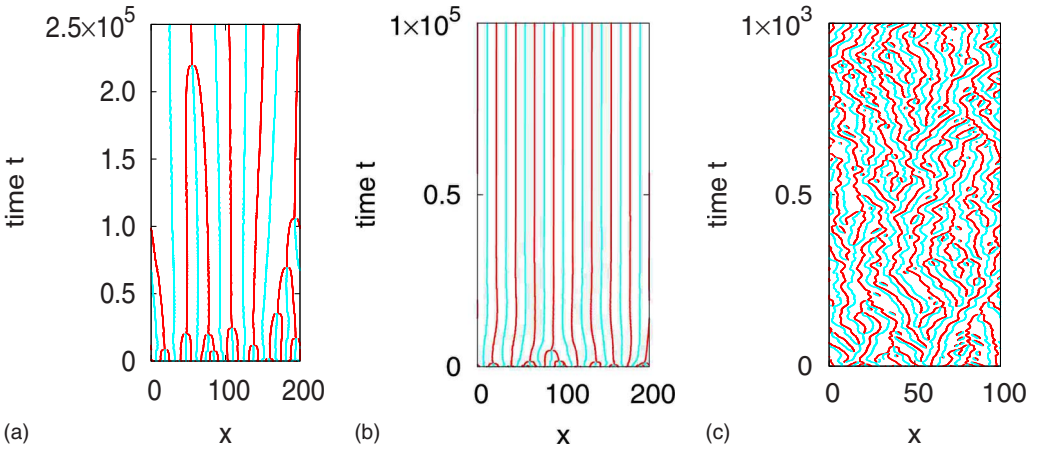

FIG. 5. (Color online) Space-time trajectories of kink [red (black)] and antikink [blue (gray)] positions obtained by numerical simulation of Eq. (7). (Left to right) $\varepsilon=0.01$: fast coarsening via kink-antikink-kink coalescence. $\varepsilon=0.1$: interrupted coarsening, fixed length scale structure as steady state. $\varepsilon=10.0$: irregular dynamics.

of kink and antikink trajectories reveals binary coalescence and annihilation of kink-antikink pairs as the dominant coarsening mechanism; see Fig. 3 for Eq. (6). Further, we find that the coarsening process is logarithmic in time, $\mathcal{L}_{\mathcal{M}} \approx \ln t$.

For the attachment-detachment dynamics, the surface morphology for $0<\epsilon\ll 1$ preserves, to leading order, the annealed morphology of faceted hill-valley structure. However, the spatiotemporal structure is dramatically different, with a specific ternary coalescence of phase boundaries, wherein two kinks simultaneously meet an antikink resulting in a kink being the sole coarsening mechanism, see Fig. 4 (left). This behavior has previously been predicted in the long-wave approximation [18] and is referred to as a kink-ternary event. Periodic structure emerge for $\varepsilon\sim 1$; see Fig. 4 (middle), while increasing the growth strength further $\varepsilon\gg 1$, one observes rough surfaces comprised of orientations $\theta\sim 0$. Further, plotting the space-time trajectories for the local minima (kinks) and maxima (antikinks) one finds an irregular (chaotic) space-time structure, see Fig. 4 (right), which also reveals kink-ternary coarsening as well as a unique ternary nucleation event, wherein an antikink bifurcates into a kink centered between two antikinks. Qualitative similar results for the three regimes are obtain by numerical simulations in the long-wave approximation; see, e.g., Refs. [7,8].

For the surface diffusion dynamics given by Eq. (7), the qualitative behavior is similar; see Fig. 5 for the three different regimes of fast coarsening, periodic structures, and spatiotemporal chaos. A significant difference is the lower value for the nondimensional driving force ε to form periodic structures. Similar results, at least for the fast coarsening

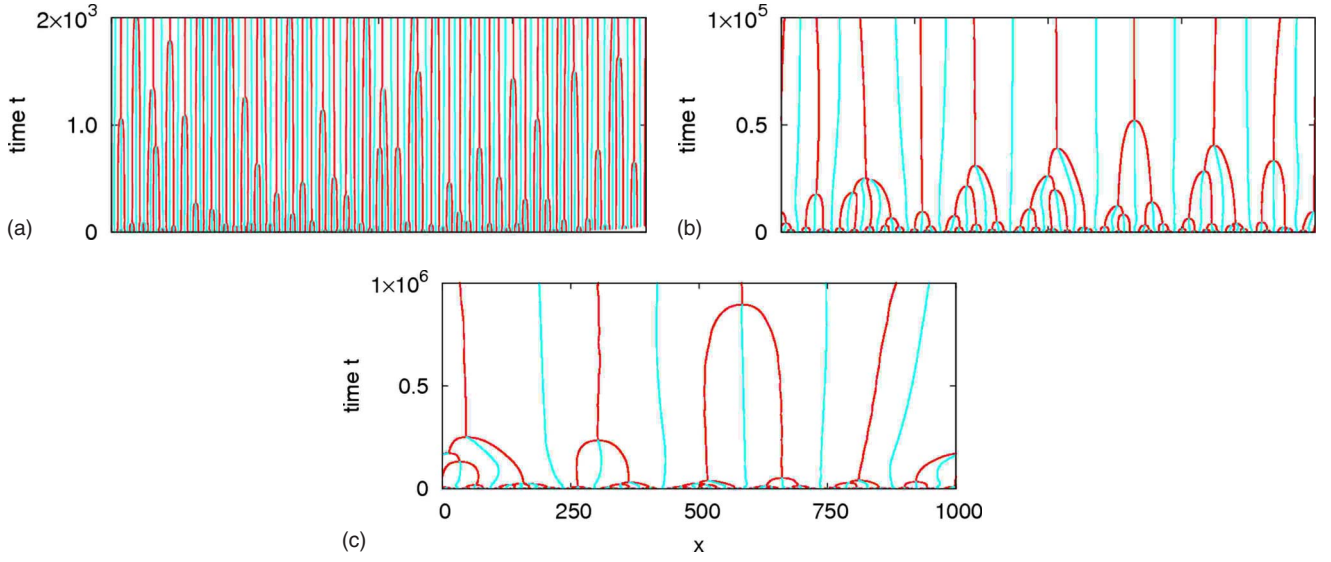

FIG. 6. (Color online) Space-time trajectories of kink [red (black)] and antikink [blue (gray)] positions obtained by numerical simulation of Eq. (6) with $\varepsilon=0.1$.

regimes have been obtained within a long-wave approximation in Ref. [9].

IV. THE FAST COARSENING REGIME

In the following we will point out quantitative differences to the long-wave approximation in the case of attachment-detachment kinetics, and will therefore focus on the late-stage fast coarsening regime of Eq. (6), which emerges when $0<\varepsilon\ll 1$. Large scale simulations, see Fig. 6 for a typical example, suggest a power law $\mathcal{L}_{\mathcal{M}}\approx ct^{1/2}$ for the morphological length scale $\mathcal{L}_{\mathcal{M}}$, as depicted in Fig. 7. Similar scaling laws have also been obtained within a long-wave approximation in Ref. [7]; however, as we will point out the prefactor significantly differs.

The following analysis has been explained to us by Watson [19]. Recall that numerical simulation reveals solutions displaying two disparate length scales at late times. Namely, the outer scale of extended near facets wherein the surface slope is approximately constant, $\theta\sim\pm\beta$, which meet and merge over a relatively narrow rounded corner inner scale. We rewrite Eq. (4) with respect to the outer scale $s=\varepsilon S$, the slow time scale $\tau=\varepsilon^3 t$, and then transform to a frame of reference moving vertically $\theta=\pi/2$, with (slow outer) speed $V=\frac{1}{\cos\beta}$ yielding

$$\varepsilon\mathcal{V}_n=\Gamma(\theta)\kappa-\varepsilon^2\left(\kappa_{SS}+\frac{1}{2}\kappa^3\right)+\left(1-\frac{\cos\theta}{\cos\beta}\right). \tag{8}$$

The outer-scale structure of the solution surface $\mathcal{I}_\varepsilon$ is approximated, to leading order, by the piecewise-affine surface $\mathcal{I}$, hereby parametrized by $\theta^{(0)}(s,\tau)=(-1)^i\beta$, $s\in[s_i(\tau),s_{i+1}(\tau)]$; here s is an arc-length parametrization of $\mathcal{I}$, and $L_i=s_{i+1}(\tau)-s_i(\tau)$ is the length of the ith facet. Now, the slope constraint $\theta^{(0)}=\pm\beta$ implies that the kinematics of the faceted surface $\mathcal{I}$ is captured by specifying the instantaneous normal velocity $\mathcal{V}_i$ of the ith facet; we presume nucleation of new facets is precluded. Now, we assume an outer expansion of the form $\theta=\theta^{(0)}(s,\tau)+\varepsilon\theta^{(1)}(s)+O(\varepsilon^2)$. This automatically solves Eq. (8) to leading order, while at order $O(\varepsilon)$ we obtain on the ith facet

$$\mathcal{V}_i=\Gamma(\beta)\theta_s^{(1)}+(-1)^i\tan\beta\theta^{(1)}. \tag{9}$$

To obtain boundary conditions on $\theta^{(1)}$ we examine the inner structure of the solution θ centered on the moving vertices $\mathcal{I}$.

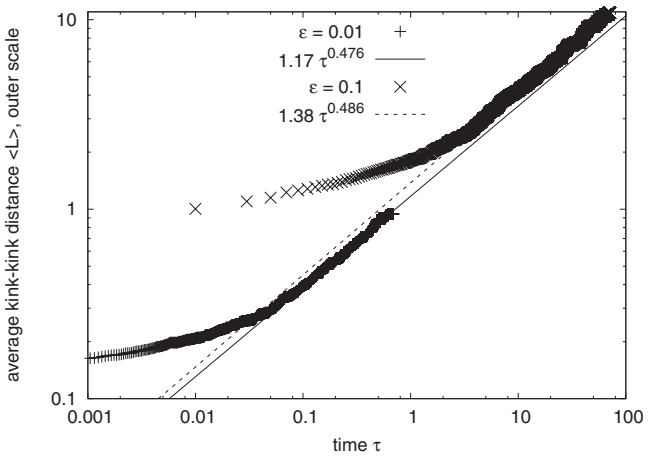

FIG. 7. Average kink-kink distance $\mathcal{L}_{\mathcal{M}}$ versus time $\tau=\varepsilon^3 t$. The data are obtained by averaging over five runs of solving Eq. (6) with initially ~100 kinks. An affine linear fit at late times reproduces the predicted scaling law $\mathcal{L}_{\mathcal{M}}\approx c\tau^{1/2}$.

Assuming an asymptotic expansion of the form $\theta=\Theta_0(S,\tau)+\varepsilon\Theta_1(S,\tau)+O(\varepsilon^2)$ yields, upon insertion into Eq. (8) and gathering together terms of order $O(1)$,

$$\Gamma(\Theta_0)\frac{d\Theta_0}{dS}-\left[\frac{d^3\Theta_0}{dS^3}+\frac{1}{2}\left(\frac{d\Theta_0}{dS}\right)^3\right]=0. \tag{10}$$

One easily finds, from applying elementary geometric identities [20], the first integral

$$K=\frac{d\Theta_0}{dS}=\sqrt{2\left[\gamma(\Theta_0)-\gamma(\beta)\frac{\cos\Theta_0}{\cos\beta}\right]}.$$

At $O(\varepsilon)$ we have

$$\frac{d}{dS}[\Gamma(\Theta_0)\Theta_1]-\left[\frac{d^3\Theta_1}{dS^3}+\frac{3}{2}\left(\frac{d\Theta_0}{dS}\right)^2\frac{d\Theta_1}{dS}\right]=1-\frac{\cos\Theta_0}{\cos\beta}.$$

Letting $\pm\Lambda$ denote the asymptotic value of the symmetric time-independent solution $\Theta_1(S)$, $\Theta_1(\pm\infty)=\pm\Lambda$, we numerically find $\Lambda=0.119$. Matching the inner-outer structure of θ we conclude

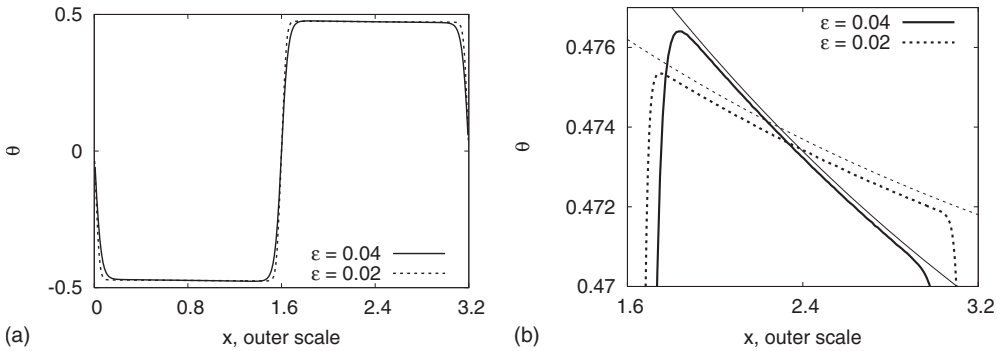

FIG. 8. Comparison of kink-antikink steady states as approached in the simulations (thick lines) of Fig. 9 and the $O(\varepsilon)$ outer solution (thin lines).

$$\theta^{(1)}[s_i(\tau)^+] = \Lambda \quad \text{and} \quad \theta^{(1)}[s_{i+1}(\tau)^-] = -\Lambda. \tag{11}$$

The solvability of Eq. (9) subject to Eq. (11) automatically yields

$$\mathcal{V}_i = \Lambda \tan\beta \left\{ 1 + 2\left(\exp\left[\frac{\tan\beta}{\Gamma(\beta)} \mathcal{L}_i \right] - 1 \right)^{-1} \right\}. \tag{12}$$

This intrinsic characterization of the facet velocities $\mathcal{V}_i$ uniquely identifies the evolution between coarsening events of the leading-order piecewise-affine surface $\mathcal{I}$, a so-called piecewise-affine dynamic surface (PADS) [21]. It will be convenient to recast this PADS in terms of an equivalent coarsening dynamical system (CDS) [18] for the evolution of the projection x_i of the ith vertex of $\theta^{(0)}$. One finds

$$\dot{x}_i = \frac{(-1)^i}{\sin\beta} \Lambda [\hat{J}(x_{i+1} - x_i) - \hat{J}(x_i - x_{i-1})], \tag{13}$$

where $\hat{J}(L) := (\exp[\frac{\tan\beta}{\Gamma(\beta)}\mathcal{L}] - 1)^{-1}$. This is the geometric extension of the long-wave theory developed in Ref. [18]. Assuming the dynamic scaling hypothesis and noting that $\hat{J}(L) \sim 1/L$ as $L \to 0+$, it follows that the asymptotic invariance of Eq. (13) under the spatiotemporal scaling $L \to \lambda L$ and $\tau \to \lambda^2 \tau$ implies the power law scaling $\mathcal{L}_{\mathcal{M}}(\tau) \sim c\tau^{1/2}$, provided $\mathcal{L}_{\mathcal{M}} \ll 1$; see Fig. 7. In particular, Eq. (13) predicts the prefactor in the power law scaling as a function of the facet angle β as $\mathcal{L}_{\mathcal{M}}(\tau) = c_{\text{stat}} c(\beta) \tau^{1/2}$, with c_{stat} a constant depending on the statistics of the initial configuration and $c(\beta)$ depending explicitly on the equilibrium Wulff slope. As pointed out in Ref. [22] the nontrivial information in scaling laws resides in the prefactor. As the obtained relation is unique to the full geometric description of the surface it further shows the limitation of the long-wave approximation if quantitative results are required. The obtained relation is not limited to the specific form of the used anisotropy function and thus provides the materials-specific information which might give insight into detailed material transport phenomena along the surface.

Stationary periodic solutions of Eq. (8) comprising of equally spaced hills (antikinks) and valleys (kinks) exist, albeit they are unstable to coarsening. We present in Fig. 8 a direct comparison of a numerically computed periodic morphology with a matched asymptotic composite solution derived from the described theory. The shape asymmetry between kink and antikink, induced by the driving force ε, is clearly well captured by the asymptotic outer solution.

Recall that the alternating-nearest-neighbor structure of Eq. (13), combined with the fact that $\hat{J}(L) \sim 1/L$ as $L \to 0+$, implies the nonexistence of binary coarsening events [18]. Furthermore, it also follows that the only possible coarsening event involves two kinks simultaneously converging on the intervening antikink with the result that a single kink emerges [18]; the so-called kink ternary. Taking therefore a periodic profile as shown in Fig. 9 as a suitable probe of the spatiotemporal coarsening, we not only confirm the convergence of Eq. (8) to the asymptotic theory (13) as $\varepsilon \to 0$, but also show the persistence of the kink ernary well beyond the range where the asymptotic theory applies.

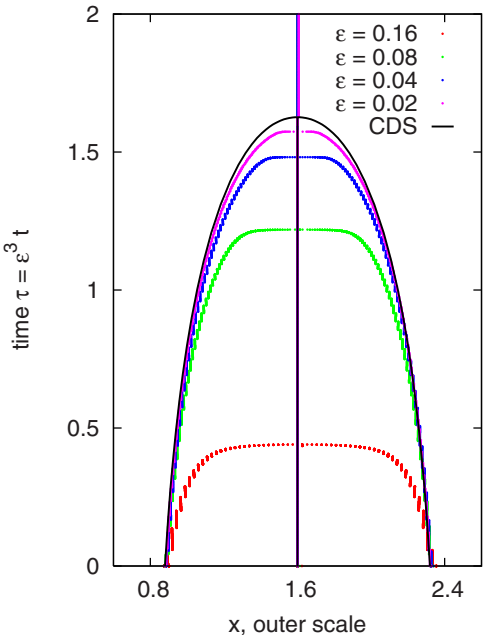

FIG. 9. (Color online) Space-time trajectories of the kink-ternary coarsening event on a periodic domain; numerical simulations of Eq. (4) for different values of ε (the height of the trajectory increases with decreasing value of ε) are compared with the solution of the CDS (uppermost curve) given in Eq. (13).

V. CONCLUSIONS

In conclusion, for driven geometric surface evolution problems we have delineated, in terms of the driving force strength ε, four distinct spatiotemporal regimes. Our results qualitatively confirm that the spatiotemporal structure of the associated long-wave theories persists into the large-slope regime. Further, we have theoretically characterized, via a matched asymptotic analysis, the piecewise-affine dynamic surface (PADS) associated with the accelerated coarsening regime $0 < \varepsilon \ll 1$ in the case of attachment-detachment kinetics. The PADS predicts the scaling law $\mathcal{L}_{\mathcal{M}} = c_{\text{stat}} c(\beta) t^{1/2}$ with a universal scaling exponent and a computed prefactor which depends explicitly on the equilibrium Wulff slope β. Extending these results for 2D surfaces and/or computing the bulk effects are problems which warrant further study. Possible numerical approaches have been developed in Refs. [23,24].

ACKNOWLEDGMENTS

We would like to thank S. J. Watson for explaining the asymptotic analysis [19] to us and for many helpful discussions. A.V. was supported by EU STRP Grant No. 016447 and NSF DMR Grant No. 0502737 within the project "MagDot" and by DFG SFB Grant No. DFG SFB 609 TP C10.

[1] J. Tersoff, B. J. Spencer, A. Rastelli, and H. von Kanel, Phys. Rev. Lett. **89**, 196104 (2002).
[2] E. Fried and M. E. Gurtin, Adv. Appl. Mech. **40**, 1 (2004).
[3] C. Herring, Phys. Rev. **82**, 87 (1951).
[4] A. DiCarlo, M. E. Gurtin, P. Podioguidugli, SIAM J. Appl. Math. **52**, 1111 (1992).
[5] J. Stewart and N. Goldenfeld, Phys. Rev. A **46**, 6505 (1992).
[6] F. Liu and H. Metiu, Phys. Rev. B **48**, 5808 (1993).
[7] A. A. Golovin, S. H. Davis, and A. A. Nepomnyashchy, Phys. Rev. E **59**, 803 (1999).
[8] A. A. Golovin, A. A. Nepomnyashchy, S. H. Davis, and M. A. Zaks, Phys. Rev. Lett. **86**, 1550 (2001).
[9] T. V. Savina, A. A. Golovin, S. H. Davis, A. A. Nepomnyashchy, and P. W. Voorhees, Phys. Rev. E **67**, 021606 (2003).
[10] D. Knoppik and A. Losch, J. Cryst. Growth **34**, 332 (1976).
[11] J. Heffelfinger and C. Carter, Surf. Sci. **389**, 188 (1997).
[12] N. Reinecke and E. Taglauer, Surf. Sci. **454**, 94 (2000).
[13] B. Li, J. Lowengrub, A. Rätz, and A. Voigt, Commun. Comput. Phys. (to be published).
[14] N. V. Medhekar, V. B. Shenoy, J. B. Hannon, and R. M. Tromp, Phys. Rev. Lett. **99**, 156102 (2007).
[15] F. Haußer and A. Voigt, Appl. Math. Lett. **19**, 691 (2006).
[16] F. Haußer and A. Voigt, Interfaces Free Boundaries **7**, 353 (2005).
[17] F. Haußer and A. Voigt, J. Cryst. Growth **275**, e47 (2005).
[18] S. J. Watson, F. Otto, B. Y. Rubinstein, S. H. Davis, Physica D **178**, 127 (2003).
[19] S. J. Watson (unpublished).
[20] B. J. Spencer, Phys. Rev. E **69**, 011603 (2004).
[21] S. J. Watson and S. A. Norris, Phys. Rev. Lett. **96**, 176103 (2006).
[22] J. Krug, Physica A **340**, 647 (2004).
[23] M. Burger, F. Haußer, C. Stöcker, A. Voigt, J. Comput. Phys. **225**, 183 (2007).
[24] S. Torabi, J. Lowengrub, A. Voigt, S. Wise, Proc. R. Soc. London, Ser. A (to be published).